*Mapana – Journal of Sciences*
2025, Vol. 24, No. 1, 23-40
ISSN 0975-3303 | https://doi.org/10.12723/mjs.72.2

# Photocatalytic and antibacterial properties of carbonaceous materials coupled NiO nanocomposites

N. Manjula*, Z. Delci†, M. Karthika‡, C. Kayathiri§, A.R. Balu*, N. Arunkumar#, V. Rajamani*, K. Devendran*, M. Sriramraj*, A. Vinith*

## Abstract

The photocatalytic and antibacterial characteristics of pure NiO (NO), GO, and rGO-integrated NiO (GNO and rNO) nanoparticles have been compared in this work. Through the process of chemical precipitation, NO and GNO NPs were created. Through the use of *Centella asiatica* leaf extract to reduce graphene oxide to rGO, rNO NC was produced utilising a one-pot green synthesis technique. The cubic crystal structure of all the samples shows a clear preferential growth along the (2 0 0) direction. Graphene oxide and reduced graphene oxide blending have a detrimental effect on the crystalline quality of NO. Reduced band gaps for the GNO and rNO samples were observed, resulting from charge delocalisation from electronic interaction between NiO and GO/rGO. The degradation efficiencies of NO, GNO and rNO catalysts were 78, 83 and 92 %, respectively, against rhodamine B after 90 min of light irradiation. The size and capacity to produce reactive oxygen species distinguish NO, GNO, and rNO NPs' antibacterial qualities. Due to decreased crystallite size, more ROS are generated for rNO, and hence enhanced antibacterial potency has been realised.

* Department of Physics, AVVM Sri Pushpam College (Affiliated to Bharathidasan University, Tiruchirappalli), Poondi, Tamilnadu, India; manjula_msc@rediffmail.com, arbalu757@gmail.com, Sruthirithi14@gmail.com, devendran2187@gmail.com, Sriramrajphysics@gmail.com, vinithakt2000@gmail.com

# Department of Physics, Anjalai Ammal Mahalingam Engineering College (Affiliated to Anna University), Kovilvenni, Tamil Nadu, India.

† Department of Physics, Dwaraka Doss Goverdhan Doss Vaishnav College, Chennai, India

‡ Department of Physics, Bon Secours College for Women, Thanjavur, India

§ Department of Physics, Annai Vailankanni Arts and Science College, Thanjavur, India

**Keywords:** Reduced graphene oxide; precipitation; XRD; photodegradation; antibacterial

## 1. Introduction

Presently, the discharges from textile industries and printing mills have made water bodies unfit for consumption due to the contamination caused by organic pollutants and their waste products [1]. In addition, the environment is contaminated by noxious and perilous substances found in the waste generated by petroleum refineries, coal conversion processing, pesticides, and drug production [2]. Reverse osmosis, flocculation, coagulation, and electrochemical oxidation are some of the various techniques used in recent years to cleanse contaminated water. However, organic pollutants display a high level of resistance due to their outstanding ability to withstand microbial attack, chemicals, temperature, and light. Recent research indicates that the use of metal oxide semiconductors in photocatalysis is a viable and hopeful method for breaking down organic contaminants into harmless substances [3]. Also, the existence of diverse bacteria and protozoan parasites serves as a notable means for human diseases. Due to the increased occurrence of novel infections and the development of bacterial resistance to antibiotics, recent research has focused on creating new antimicrobial drugs [4]. The bacteria's resistance stems from its cell wall, which offers strength, stiffness, and shape in the face of mechanical damage and osmotic rupture. It has been proved that nanosized metal oxide semiconductors have better efficacy while treating bacteria and the infectious diseases caused by them [5]. Photoactivation, concentration, shape, size, and chemical composition of nanoparticles determine their antibacterial efficacy.

Photocatalytic and antimicrobial applications extensively employ a range of metal oxide semiconductors, including ZnO, CdO, $TiO_2$, $SnO_2$, MgO, and others. Nickel oxide (NiO), a p-type semiconductor with a band gap of 3.6-4.0 eV, has many possible uses as a photocatalyst, in battery electrodes, as gas sensors, in electrochemical devices, and more, because of its unique features, such as its effects on volume, surface, and quantum size [6]. Because of its low cost, long-term stability, and non-toxicity, nickel oxide (NiO) is an excellent antibacterial agent and highly effective at eliminating environmental pollutants from wastewater [7]. For electrochemical investigation, NiO exhibits remarkable electron-transfer characteristics and a substantial active surface area [8]. Despite its excellent use in photocatalytic and antibacterial applications, the efficacy of NiO is significantly diminished due to the following described issues: i) The material has a wide band gap, which means it can only absorb a small portion of sunlight's spectrum. ii) It does not transmit light well. iii) It has a tendency to clump together. iv) It does not disperse easily. v) It forms complexes with metal ions that undergo redox reactions. vi) There is a high rate of recombination between

electrons and holes. There is room for advancement in this area due to the aforementioned shortcomings.

rGO and graphene oxide GO are carbonaceous materials exhibiting amazing properties like high surface area, room temperature electron mobility, and outstanding thermal, mechanical, electrical, and optical characteristics. These properties make them highly promising for various applications. It is believed that incorporating GO and rGO into the NiO matrix could address the mentioned drawbacks of NiO. Thanks to its layer of carbon atoms in the form of $sp^2$ hybrid orbitals [9], GO, a two-dimensional layered carbon material, has remarkable optical, electrical, and mechanical characteristics. Composites containing NiO [10], $MnO_2$ [11], ZnO [12], and $TiO_2$ [13] have been prepared using GO as the matrix for gas-sensing supercapacitors and water splitting applications. Reduced graphene oxide with $sp^2$ as well as $sp^3$ hybridised network frame possess extraordinary characteristics which makes it behave as a semiconductor and has the potential to be utilised as a catalyst when coupled with other semiconductors [14]. Literature findings show that the combination of rGO with semiconductors such as CdS [15], PbS [16] and NiO [17] enhanced photocatalytic, electrochemical and gas sensing properties have been realised. Motivated with these results, in this work NiO, GO and rGO blended NiO NPs were synthesised. Chemical precipitation was used to make pure NiO and GO-NiO NPs. rGO-NiO hybrid was a one-pot synthesised reducing graphene oxide with leaf extract from *Centella asiatica*. *C. asiatica,* belonging to *Apiaceae* family contains pentacyclic triterpenoids, asiaticoside, brahmoside, asiatic and Bramhic acids as prominent constituents. These are in addition to amino acids, tannins, volatile oils, phytosterols, and flavanoids. Flavonoids are able to convert GO to rGO because of their hydroxyl groups. The photocatalytic, electrochemical, and antibacterial properties of NiO, GO, and rGO blended NiO nanoparticles are compared in this work.

## 2. Experimental

### 2.1 *Chemicals used*

Nickel chloride, graphene oxide powder and liquid ammonia are the chemicals used.

### 2.2 Synthesis procedure

#### 2.2.1 *NiO (NO) NPs*

NiO nanoparticles were synthesised by calcining at 300°C for 2 hours and crushing the precipitates formed after dissolving 0.1 M nickel chloride in 80 mL demineralised water and 20 mL liquid $NH_3$, then aged for 6 hours.

### 2.2.2 *GO-NiO (GNO) NC*

After ultrasonically treating 80 mL of water with 0.05 g of graphene oxide powder for 30 minutes, an evenly distributed GO solution was formed, which could then be used to synthesise GNO NC. The GO solution was mixed with 0.1 M nickel chloride and liquid $NH_3$ (20 mL), keeping the pH at 10. The solution was aged for 6 hours after being agitated for 30 minutes. The precipitates that result from this process are filtered, calcined at 300°C for 2 hours, and then pulverised.

### 2.2.3 *rGO-NiO (rNO) NC*

The reducing and capping agent *Centella asiatica* leaf extract is used to reduce graphene oxide to rGO. The leaf extract was obtained by grinding 25 g of *Centella asiatica* leaves washed with water and ethanol. 0.1 M nickel chloride and leaf extract (20 mL) were added to the GO solution obtained as described in section 2.2.2. The solution was then maintained at 90°C for 5 hours. To get rNO NC, the mixture was then filtered, thermally treated for four hours at 80°C, and crushed.

### 2.3 Characterization

NO, GNO and rNO NPs were characterised using "PW 340/60", "HITACHI S-3000H", "LAMBDA-35" and RX-1 Cary Eclipse spectrometer to evaluate their structure, morphology, optical and luminescent properties.

### 2.4 Photocatalytic test

Rhodamine B (RhB) dye was degraded using visible light utilising NO, GNO, and rNO catalysts. The dye solution was obtained by dissolving 0.05 M dye in 80 mL water. The adsorption of the dye by the catalysts was determined by maintaining the solution with the catalysts in a dark environment prior to exposure to light. On light exposure, 4 mL of the solution was taken; the catalysts were centrifuged, and absorbance spectra at $\lambda$ = 552 nm were obtained.

### 2.5 Antibacterial test

NO, GNO and rNO NPs were tested for their ability to suppress the development of *S. aureus* and *K. pneumonia* bacteria by exposing them to aan gar medium spread out in Petri dishes. To find out how well the NPs killed bacteria, 2 mg of them mixed in 25 and 50 µL of DMSO were put into the plates' open wells, and the blocking zones that formed were seen.

## 3. Results and discussion

### 3.1 *XRD*

The XRD patterns of NO, GNO, and rNO nanoparticles are illustrated in Fig. 1.

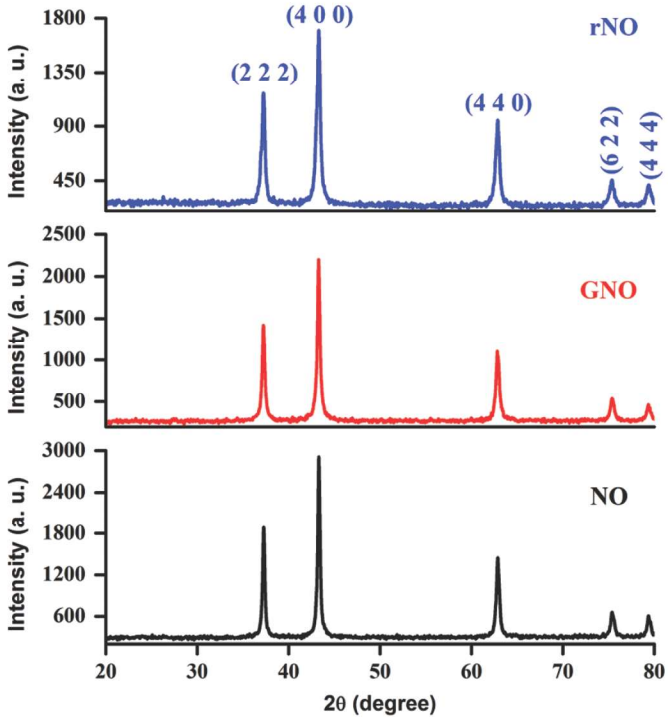


**Fig. 1:** XRD patterns of NO, GNO and rNO

The detected peaks are attributed to the cubic crystal structure of NiO, as indicated by the JCPDS Card No. 04-0835. All of the samples demonstrate a pronounced preference for development along the (2 0 0) crystallographic plane. A possible explanation for the lack of GO and rGO-related peaks in GNO and rNO XRD patterns could be the strong intensity of NiO peaks. Pure NiO's (2 0 0) peak intensity decreased with GO and rGO incorporation, confirming the deterioration of its crystalline nature by the occupancy of graphene-based materials. Compared to NiO (2.0901Å), GO-doped NiO exhibited increased d-spacing value (2.0913 Å); whereas rGO-doped NiO exhibited decreased d-spacing value (2.0899 Å). The oxidation of graphite results in the formation of oxygen-containing functional groups between layers, which may account for the observed increase in the d-spacing value for GNO [18]. The decreased d-spacing value observed for the rNO NC might be due to crystallite sizes estimated using the Scherrer equation being 39, 35 and 29 nm, respectivel,y for NO, GNO and rNO samples.

### 3.2 SEM analysis

Grains appeared to be uniformly distributed for NO, GNO and rGO as evinced from the SEM images (Fig. 2).

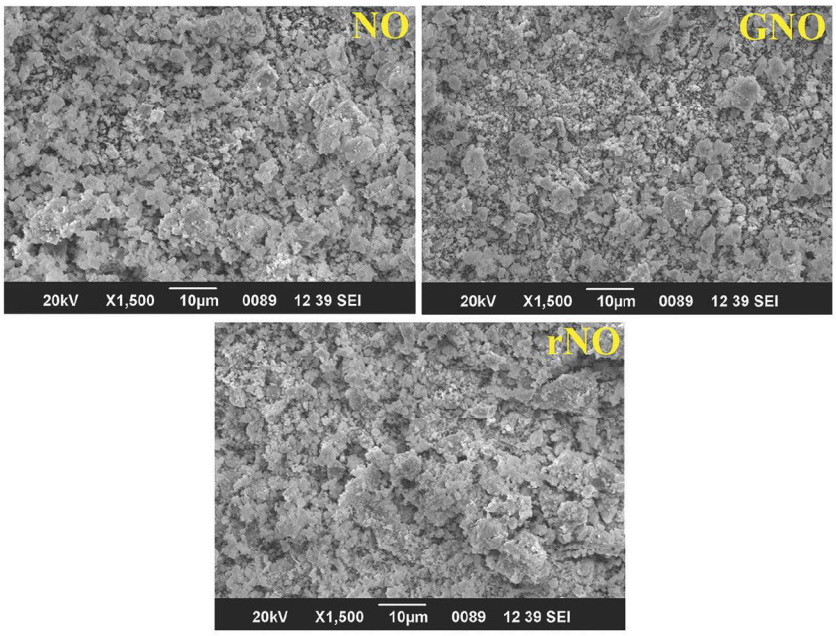


**Fig.2:** NO, GNO and rNO's SEM images

Few clustered grains are also visible. The grain size of NO decreased with GO and rGO blending.

### 3.3 Optical studies

In the UV region, NO exhibits a band-to-band absorption peak at 348 nm (Fig. 3(a)) [14]. The absorption peak got red-shifted to 357 nm for GNO and to 351 nm for rNO. Both GNO and rNO exhibited higher absorption, which might be due to the absorbing ability of GO and rGO sheets. The red shift suggests decreased band gap energies ($E_g$) for both GNO and rNO samples. The $E_g$ values calculated from Fig. 3(b), were3.47, 3.4, and 3.35 eV for NO, GNO and rNO samples, respectively.

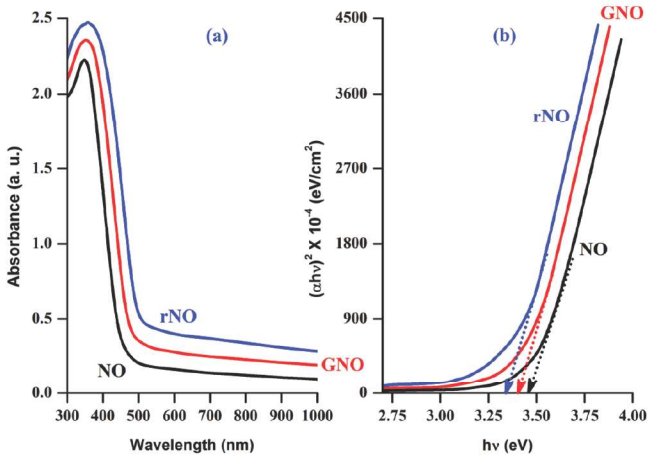


**Fig.3: a) Absorption spectra, b) Tauc plots of NO, GNO and rNO**

The charge delocalisation resulting from the electrical interaction between NiO and GO/rGO may be the cause of the reduced band gap values seen for both GNO and rNO samples. rNO sample's improved light absorption capacity and smaller band gap allowed it to function better photocatalytically.

## 3.4 FTIR

In the FT-IR spectra of NO, GNO, and rNO (Fig. 4), the peak at 3423 $cm^{-1}$ corresponds to the O-H stretching vibration of inter-layer water molecules [19]. The vibrations of the OH group that are implicated in significant hydrogen bonding may be assigned to the peaks at 2923 and 2854 $cm^{-1}$ [20]. The carboxylic acid group's –C=O bond exhibits a peak at 1702 $cm^{-1}$. Water molecule bending vibration [19] determines the 1632 $cm^{-1}$ peak. O–C=O symmetric stretching from the adsorption of ambient $CO_2$ is assigned the peak at 1384. Observed at 1029 $cm^{-1}$ for NO, GNO, and at 1033 for rNO [14] is C–O stretching vibration.

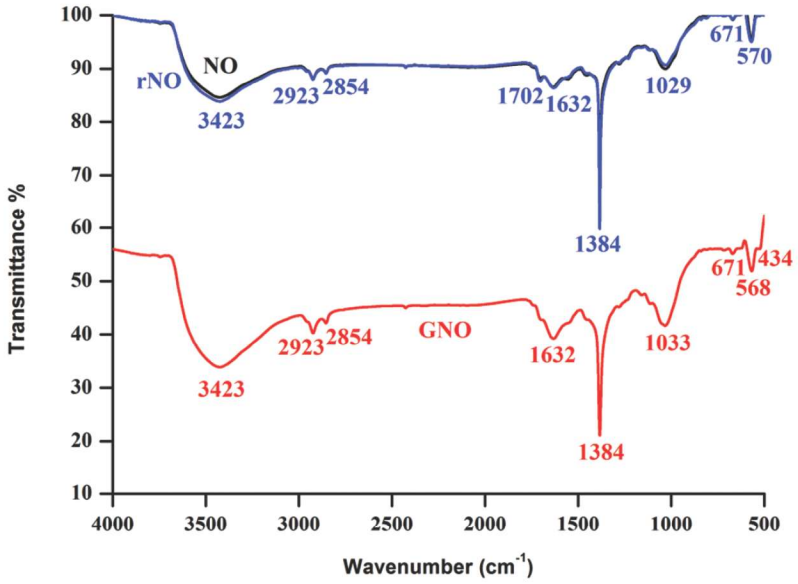


**Fig.4:** FTIR spectra of NO, GNO and rNO

The δ Ni–O–H vibration is the cause of the 671 band [21]. Absorption bands from 570 to 434 $cm^{-1}$ correspond to Ni-O stretching [22]. The rNO sample's 434 $cm^{-1}$ peak is the transverse optical mode caused by the $Ni^{2+}$ sublattice's 180° displacement opposite the $O^{2-}$ sublattice [23].

## 3.5 Raman

Raman spectra of NO, GNO, and rNO NPs are displayed in Fig. 5. At 500 $cm^{-1, a}$ vibrational band of NiO corresponding to one phonon 1P transverse optical (TO) mode was found [24].

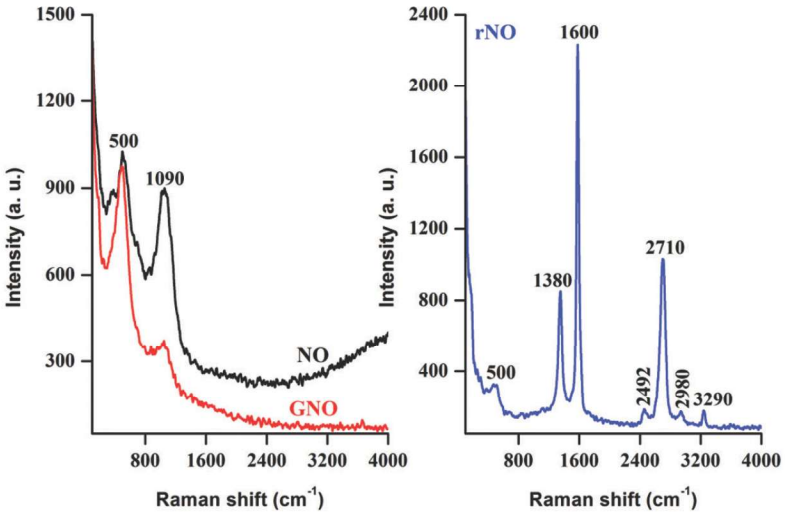


**Fig.5:** Raman spectra of NO, GNO and rNO

The vibrations of Ni-O resulted in the 2L0 mode at 1096 $cm^{-1}$ for NO and GNO [25]. rNO's D, G and 2D bands at 1389, 1600 and at 2710 correspond to defects/disorders, $sp^2$ graphite structure, and second order two phonon process [26].

## 3.6 PL

PL spectra of NO, GNO and rNO are shown in Fig. 6. When electrons moved from the shallow donor level created by Ni interstitials to the shallow acceptor level created by Ni vacancies, the 494 nm peak was emitted [27].

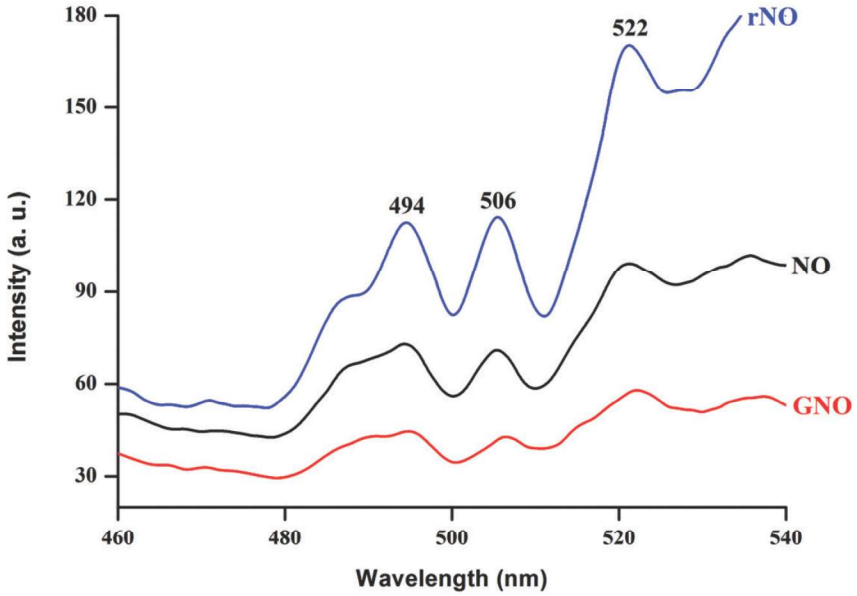


**Fig.6:** PL spectra of NO, GNO and rNO

The 506 nm emission peak is generated by electron-hole recombination at the imperfection site [28]. The signal at 522 nm is due to recombination centres, which can be extrinsic or intrinsic vacancies or point defects [29]. The rNO nanocomposite's reduced PL intensity may be attributed to the interfacial charge transfer from NiO NPs to rGO sheets [30]. After adding rGO sheets, the PL intensity of NiO significantly decreased, which suggests decreased $e^-/h^+$ radiative recombination. Here, rGO sheets trap NiO's photogenerated electrons, blocking their interaction with holes, improving photocatalytic activity [14].

## 3.7 Photocatalytic activity

Fig. 7(a-c) confirms the degradation nature of the catalysts, as the intensities of the RhB absorption peak diminish as the irradiation time increases. Compared to NO, GNO and rNO catalysts exhibit good photocatalytic decomposition characteristics, with rNO showing superior photocatalytic activity. GO and rGO contain oxygen-containing functional groups, creating charged nucleophilic centres that form π-π linkages with adsorbates. This attracts cationic dyes like RhB to GNO and rNO catalysts through oppositely charged interactions, resulting in increased photodegradation efficiency [31].

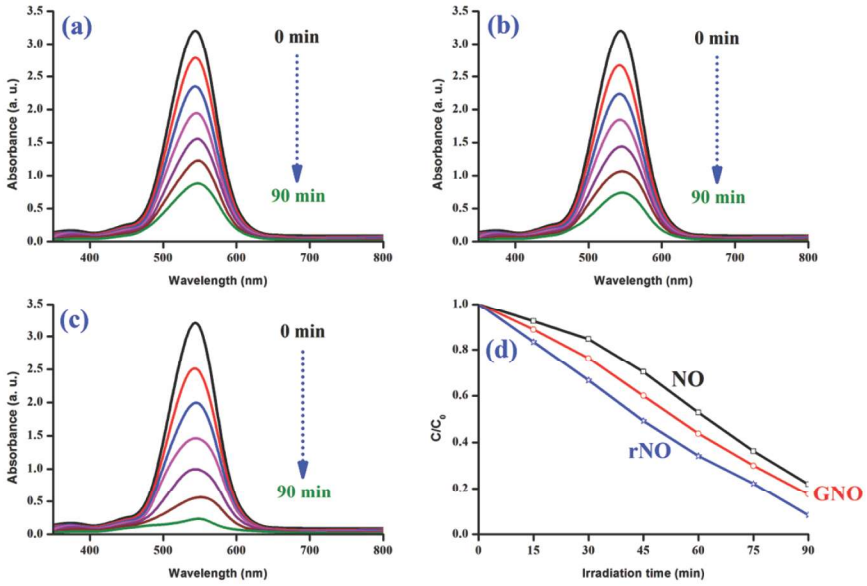


**Fig.7:** (a-c) Absorbance vs irradiation time, and d) $C/C_0$ vs irradiation time plot of RhB by NO, GNO and rNO

Figure 7(d) shows the rates of photodegradation for each sample. The dye degradation rate of pure NiO rose progressively ($C/C_0$ vs time) with GO and rGO mixing, possibly due to rapid electron transfer between NiO and GO/rGO without recombination. The improved breakdown efficiency of GNO and rNO is likely due to their large surface area, superior electron transport

capacity, and reduced photocatalyst aggregation [32]. The degradation efficiencies of NO, GNO and rNO catalysts calculated after 90 min are shown in Fig. 8. rNO's maximum degradation efficiency of 92% was attributed to effective charge separation of photo-excited electron-hole pairs between rGO and NiO, along with synergistic and molecular interactions.

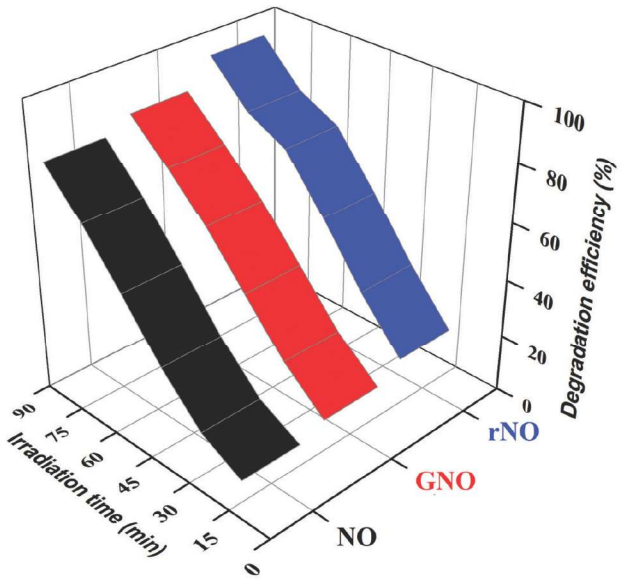


**Fig.8:** Degradation efficiencies of NO, GNO and rNO

The first order rate constants (k) calculated from the slopes of the plots (ln $C/C_0$ vs. irradiation time) were 0.0164 ($R^2$ = 0.89083), 0.01894 ($R^2$ = 0.91934) and 0.02601 $min^{-1}$ ($R^2$ = 0.93094) for NO, GNO and rNO catalysts. The value of k of rNO catalyst was found to be much higher than that of NO and GNO catalysts. Possible reasons for this are: i) large volume-to-surface ratio, ii) increased optical absorption, and iii) lowered recombination rate of photo-generated species. In addition to this, the rGO induces quantisation of the NiO NPs, leading to notable quantum effects. Table 1 compiles a comparison of the rNO catalyst's degrading efficiency with previously published data.

**Table 1**

Comparison of rNO catalyst's degrading efficiency with earlier published rGO-based catalysts

| Catalyst | Light | Reaction time (min) | Dye | Degradation efficiency | Reference |
|---|---|---|---|---|---|
| rGO -ZnO | UV | 150 | RhB | 93% | [33] |
| rGO- $TiO_2$ | UV | 21 | RhB | 75% | [34] |

| | | | | | |
|---|---|---|---|---|---|
| rGO-$AgFeCo_2O_4$ | Solar | 120 | RhB | 86% | [35] |
| rGO- $TiO_2$CdO-ZnO-Ag | UV | 15 | Methylene blue | 91% | [32] |
| rGO- CdO | UV | 110 | Methylene blue | 80% | [36] |
| rGO- NiO | Visible | 90 | RhB | 92% | Present work |

Figure 9 illustrates the process of photocatalytic degradation of RhB dye using NiO, GO-NiO, and rGO-NiO nanoparticles when exposed to visible light. The $e^-$ of VB moves to CB when the mixed solution of dye and catalysts is exposed to visible light. This process results in the formation of $O_2^{*-}$ radicals through a reaction with $O_2$. Conversely, the $OH^-$ in aqueous solution occupies the pores in the VB to generate $OH^*$ radicals, which oxidise RhB, decomposing into $CO_2$ and $H_2O$. Because of its weak ability to absorb visible light, pure NiO has a high band gap value, which severely limits its catalytic efficacy.

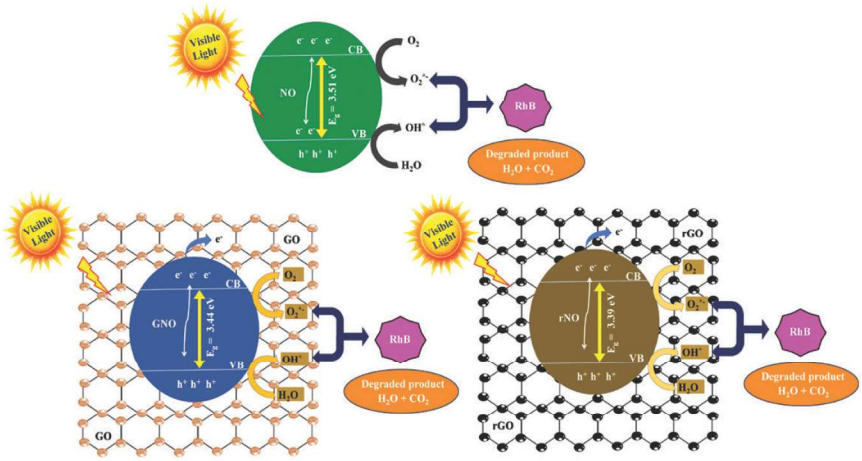


**Fig.9:** Diagram showing the photocatalytic activity of NO, GNO, and rNO catalysts mediated by visible light

Pure NiO's visible light absorption is enhanced by GO and rGO ornamentation. Also, $e^-/h^+$ pairing recombination was slowed down with the addition of GO and rGO sheets. The delayed recombination period of photogenerated $e^-/h^+$ couples in NiO increases free charge carrier density in dye solutions with GNO and rNO catalysts. Further reactions between these extra charge carriers and the $O_2$ and $OH^-$ in the mixed solution formed $O_2^{*-}$ and $OH^*$ radicals, which degrade RhB dye more quickly than pure NiO. Reduced crystallite size, increased surface-to-volume ratio, and less aggregation of NiO NPs could be the causes of rNO catalyst's notable improvement in degrading capacity.

Radical scavenging assays were conducted (Fig. 10) using 2 mM benzoquinone, benzoic acid, and EDTA to discover the radicals that predominated the photocatalytic activity of the rNO catalyst, serving as scavengers for $OH^*$, $O_2^{*-}$, and $h^+$, respectively. Without scavengers, a maximum degradation efficiency of 98.3% was achieved. The decrement in the degradation efficiencies observed with scavenger addition suggested their dominance in the degradation process. The order of degradation efficiencies achieved with the scavengers is represented as $O_2^{*-} > OH^* > h^+$.

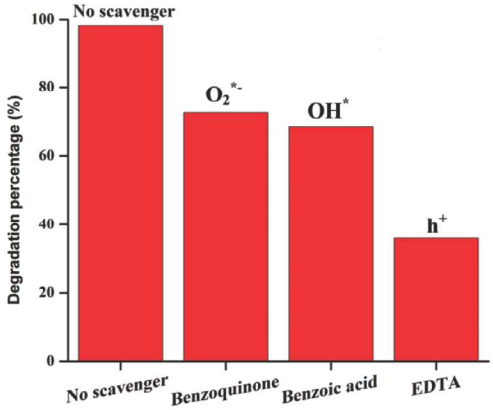


**Fig. 10:** rNO catalyst's scavenger test

A key part of making a good photocatalyst is making sure that the nanoparticles' structures stay stable and can be used again and again. rNO catalyst was subjected to recycling tests to confirm its stability. After every cycle (90 min), the catalyst was collected, washed and dried. Following the catalyst's dispersion into a new RhB dye solution, the dye degradation analysis was conducted five times, and the results are shown in (Fig. 11(a)). The catalyst did not show any appreciable decrement in efficiency up to five cycles, confirming its more stable nature. As a mark of evidence,the recycled catalyst's XRD (Fig. 11(b)) confirmed no structural modifications and resembled the same as given in Fig. 1.

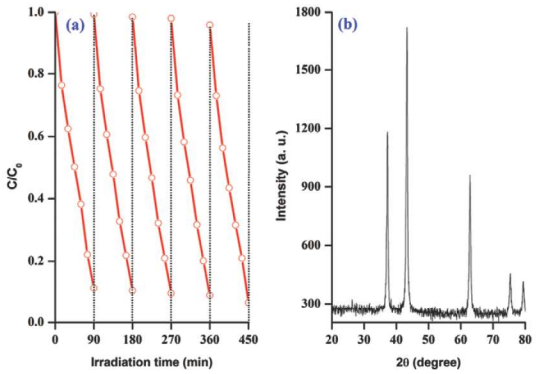


**Fig. 11:** a) Recycle tests of rNO catalyst, b) XRD pattern of the recycled catalyst

### 3.8 Antibacterial activity

The zones of inhibition that the NO, GNO, and rNO NPs created around the *S. aureus* and *K. pneumoniae* bacteria are displayed in Fig. 12, and Table 2 lists their respective values. All the synthesised NPs effectively resisted the growth of the tested pathogens, and the order of inhibition rate is represented as rNO> GNO >NO.

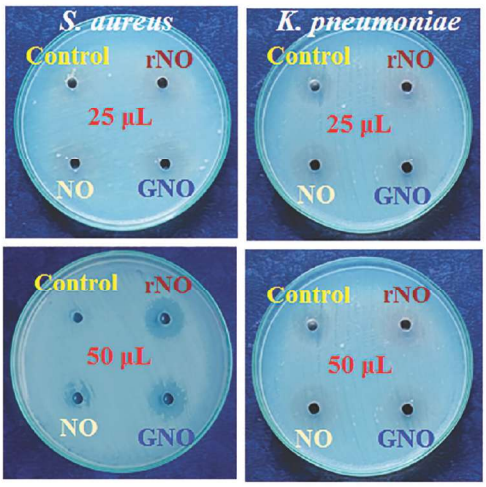


**Fig.12:** Antibacterial activity of NO, GNO and rNO against a) *S. aureus* and b) *K. pneumoniae bacteria*

The antibacterial activity of NO, GNO and rNO relies on the following factors:

i) cellular uptake, ii) ion dissolution and iii) reactive oxygen species generation [37]. Bacterial cell death was produced by the accumulation of NO, GNO, and rNO NPs on the cytoplasmic liquid membrane, as well as NP-induced membrane rupture. Nanoparticles impede cellular metabolism and DNA replication due to their affinity for protein, phosphate, and nitrogen. The production of reactive oxygen species triggers oxidative stress, which in turn damages cells [38]. $Ni^{2+}$ ions from NPs damage bacteria by interacting with phosphorus and sulfur-containing DNA. The liberated $Ni^{2+}$ ions inhibit DNA replication and inactivate proteins, killing bacteria [39]. NO, GNO, and rNO NPs may differ in antibacterial action due to size and ROS production. GNO and rNO's smaller crystallite sizes promote biomolecule absorption and cellular impact. ROS production increases significantly due to decreasing crystallite size, which breaks the bacterial cell membrane. Increased metal ion absorption into bacterial cell membranes, caused by GO and rGO decorating, changes membrane permeability and leads to protein leakage [40]. Graphene-based nanoparticles have been documented in the literature to be able to decrease mitochondrial membrane potential, leading to an increase in ROS generation and, ultimatel,y the deactivation of the mitochondrial pathway, which kills the bacteria [41]. Table 2 infers that all

the synthesised NPs showed significant resistance against *S.aureus* bacteria better than *K. pneumonia* bacteria. The absence of an outer lipid membrane in gram-positive bacteria makes their thick peptidoglycan layer more vulnerable to damage.

**Table 2**

**ZOI values observed for NO, GNO and rNO against *S. aureus* and *K. pneumoniae* bacteria**

| Sample | Zone of inhibition (mm) | | | |
|---|---|---|---|---|
| | 25 µL(DMSO) | | 50 µL (DMSO) | |
| | *S. aureus* | *K. pneumoniae* | *S. aureus* | *K. pneumoniae* |
| NO | 5 | 3 | 7 | 5 |
| GNO | 10 | 9 | 14 | 12 |
| rNO | 15 | 12 | 18 | 15 |

## 4. Conclusion

NiO (NO), GO, and rGO blended NiO (GNO and rNO) NPs were successfully synthesised. Their photocatalytic and antibacterial nature was evaluated in addition to their structural and optical properties. NO, GNO and rNO exhibited cubic crystal structure. Blending GO and rGO enhanced NiO's visible light-absorbing capacity. The contribution of GO and rGO reduced NO's band gap from 3.47 to 3.4 and 3.35 eV, respectively. Photodegradation efficiencies of NO, GNO and rNO catalysts against the degradation of RhB dye were 78, 83 and 92%, respectively. Blending GO and rGO significantly enhanced NiO's ability to prevent bacterial growth. The rGO-embedded NiO was found to have superior catalytic and antibacterial properties based on the obtained results, making it a viable option for the aforementioned applications. Also, in future, by utilising rNO nanocomposite, energy harvesting and storage, which is a challenging issue to meet the increasing demand of energy consumption, could be achieved with high performance with minimal energy loss.

## 5. Acknowledgements

The XRD, PL, and Raman results were greatly appreciated by Alagappa University, Karaikudi.

## "Statements and Declarations

### Funding

The authors declare that no funds, grants, or other support were received during the preparation of this manuscript.

## Competing Interests

The authors have no relevant financial or non-financial interests to disclose.

## Conflict of Interest

On behalf of all authors, the corresponding author states that there is no conflict of interest."

## "Author's contribution

**Conceptualization** – N. Manjula; **Data curation** – Z. Delci; **Formal analysis** – M. Karthika; **Funding acquisition** – C. Kayathiri; **Investigation** – A.R. Balu; **Methodology** – N. Arunkumar; **Project administration** – A.R. Balu; **Resources** – K. Devendran; **Software; Supervision** – V. Rajamani; **Validation** – M. Sriramraj; **Visualization** – A. Vinith; **Roles/Writing - original draft** – A.R. Balu; **Writing - review & editing** – A.R. Balu."

## References

[1]. N. Ajoudanian andA. Nezamzedeh-Ejhieh, "Enhanced photocatalytic activity of nickel oxide supported on clinoptilolite nanoparticles for the photodegradation of aqueous cephalexin," Mater. Sci. Semicond. Proc, vol. 36, p.162, 2015. https://doi.org/10.1016/j.mssp.2015.03.042.

[2]. M.L. Hitchman and F. Tian, "Studies of $TiO_2$ thin films prepared by chemical vapour deposition for photocatalytic and photoelectrocatalytic degradation of 4-chlorophenol," J. Electroanal. Chem, vol. 538, p.165, 2002. https://doi.org/10.1016/S0022-0728(02)01252-4.

[3]. V.Vo, T.P.T. Thi, H.Y. Kim, and S.J. Kim, "Facile post-synthesis and photocatalytic activity of N-doped ZnO–SBA-15," J. Phys. chem. Sol, vol. 75, p. 403, 2014. https://doi.org/10.1016/j.jpcs.2013.11.011.

[4]. A.M. Fischbach, and T.C.Walsh, "Antibiotics for emerging pathogens," Science, vol. 325, p. 1089, 2009. https://doi.org/10.1126/science.1176667.

[5]. M.Vairavel, E. Devaraj, and R. Shanmugam, "An eco-friendly synthesis of Enterococcus sp.–mediated gold nanoparticle induces cytotoxicity in human colorectal cancer cells," Environ. Sci. Poll, Res, vol. 3, p. 1, 2020. https://doi.org/10.1007/s11356-019-07511-x.

[6]. A.A. Ezhilarasi, J.J. Vijaya, K. Kaviyarasu, X. Zhang and L. John Kennedy, "Green synthesis of nickel oxide nanoparticles using *Solanum trilobatum* extract for cytotoxicity, antibacterial and photocatalytic studies," Surf. Interfaces, vol. 20, p. 100553, 2020. https://doi.org/10.1016/j.surfin.2020.100553.

[7]. S.Anitha, S. Suganya, D. Prabha, S.Balamurugan and A.R. Balu, "Synthesis and characterization of NiO-CdO composite materials towards photoconductive and antibacterial applications," Mater. Chem. Phys, vol. 211, p. 88, 2018. https://doi.org/10.1016/j.matchemphys.2018.01.048.

[8]. M.Z. Iqbal and R.J.Kriek, "Silver/nickel oxide (Ag/NiO) nanocomposites produced via a citrate sol-gel route as electrocatalyst for the oxygen evolution reaction (OER) in alkaline medium," Electrocatalysis, vol. 9, p. 279, 2018. https://doi.org/10.1007/s12678-018-0455-5.

[9]. J.Gao, P. He, T.Yang, L.Zhou, X.Wang, S. Chen, H. Lei, H.Zhang, B. Jia and J. Liu, "Electrodeposited NiO/graphene oxide nanocomposite: An enhanced voltammetric sensing platform for highly sensitive detection of uric acid, dopamine and ascorbic acid," J. Electroanal. Chem, vol. 852, p.113516, 2019. https://doi.org/10.1016/j.jelechem.2019.113516.

[10]. F. Soofivand and M. Salavati-Niasari, "Step synthesis and photocatalytic activity of NiO/graphene nanocomposite under UV and visible light as an effective photocatalyst," J. Photochem. Photobiol, A Chem, vol. 337, p. 44, 2017. https://doi.org/10.1016/j.jphotochem.2017.01.003.

[11]. R.M.Obodo, H.E. Nsude, C.U. Eze, B.O.Okereke, S.C.Ezugwu, I. Ahmed, M. Maaza and F.I.Ezema, "Optimization of $MnO_2$, NiO and $MnO_2$@ NiO electrodes using graphene oxide for supercapacitor applications," Curr. Res. Green Sustain. Chem, vol. 5, p. 100345, 2022. https://doi.org/10.1016/j.crgsc.2022.100345.

[12]. K. Rahimi, A. Yazdani and M. Ahmadirad, "Graphene quantum dots enhance UV photoresponsivity and surface-related sensing speed of zinc oxide nanorod thin films," Mater. Des, vol. 140, p. 222, 2018. https://doi.org/10.1016/j.matdes.2017.12.010.

[13]. A. Bayat and E. Saievar-Iranizad, "Graphene quantum dots decorated rutile $TiO_2$ nanoflowers for water splitting application," J. Energy. Chem, vol. 27, p. 306, 2018. https://doi.org/10.1016/j.jechem.2017.09.036.

[14]. K. Rahimi, H. Zafarkish and A. Yazdani, "Reduced graphene oxide can activate the sunlight-induced photocatalytic effect of NiO nanowires," Mater. Design, vol. 144, p. 214.2018. https://doi.org/10.1016/j.matdes.2018.02.030.

[15]. L. Zou, X. Wang, X. Xu and H. Wang, "Reduced graphene oxide wrapped CdS composites with enhanced photocatalytic," Ceram. Int, vol. 42, p. 372, 2016. https://doi.org/10.1016/j.ceramint.2015.08.119.

[16]. B. M. Garcia, A. Polovitsyn, M. Prato and I. Moreels, "Efficient charge transfer in solution-processed PbS quantum dot–reduced graphene oxide hybrid materials," J. Mater. Chem. C, vol. 3, p. 7088.2015. https://doi.org/10.1039/C5TC01137J.

[17]. D. Zhang, H. Chang, P. Li and R. Liu, "Characterization of nickel oxide decorated-reduced graphene oxide nanocomposite and its sensing properties toward methane gas detection," Electron, vol. 27, p. 3723.2016. https://doi.org/10.1007/s10854-015-4214-6.

[18]. T.A. Pham, B.C. Choi and Y.T. Jeong, "Facile covalent immobilization of cadmium sulfide quantum dots on graphene oxide nanosheets: preparation, characterization and optical properties,"Nanotechnol, vol. 21, p. 465503. 2010. https://doi.org/10.1088/0957-4484/21/46/465603.

[19]. M. El-Kemary, N. Nagy and I. El-Mehasseb, "Nickel oxide nanoparticles: Synthesis and spectral studies of interactions with glucose," Mater. Sci. Semicond. Proc, vol. 16, p. 1747, 2013. https://doi.org/10.1016/j.mssp.2013.05.018.

[20]. K. Kaviyarasu, E. Manikandan, J. Kennedy, M. Jayachandran, R. Ladchumananandasiivam, U.U. De Gomes and M. Maaza, "Synthesis and characterization studies of NiO nanorods for enhancing solar cell efficiency using photon upconversion materials," Ceram. Int, vol. 42, p. 8385,2016. https://doi.org/10.1016/j.ceramint.2016.02.054.

[21]. S. Meybodi, S.A. Hosseini, M. Rezaee, S.K. Sadrnezhaad and D. Mohammadyani, "Synthesis of wide band gap nanocrystalline NiO powder via a sonochemical method," Ultrasonic Sonochem, vol. 19, p. 841, 2012. https://doi.org/10.1016/j.ultsonch.2011.11.017.

[22]. X.M. Ni, Y.F. Zhang, D.Y. Tian, H.G. Zheng and X.W. Wang, "Synthesis and characterization of hierarchical NiO nanoflowers with porous structure," J. Cryst. Growth, vol. 306, p. 418,2007. https://doi.org/10.1016/j.jcrysgro.2007.05.013.

[23]. V. Biju and M. Abdul Khadar, "Fourier transform infrared spectroscopy study of nanostructured nickel oxide,"Spectrochim. Acta A Mol. Biomol. Spectroscopy, vol. 59,p. 121, 2003. https://doi.org/10.1016/S1386-1425(02)00120-8.

[24]. M. Ben Amor, A. Boukhachem, A. Labidi, K. Boubaker and M. Amlouk, "Physical investigations on Cd doped NiO thin films along with ethanol sensing at relatively low temperature," J. Alloys Compnd, vol. 693,p. 490, 2016. https://doi.org/10.1016/j.jallcom.2016.09.207.

[25]. F.T. Thema, E. Manikandan, A. Gurib-Fakim and M. Maaza, "Single phase BunseniteNiO nanoparticles green synthesis by *Agathosmabetulina* natural extract," J. Alloys Compnd. Vol. 657, p. 655, 2016. https://doi.org/10.1016/j.jallcom.2015.09.227.

[26]. D. Graft, F. Molitor, E. Ensslin, C. Stampfer, A. Jungen, C. Hierold and L. Wirtz, "Spatially resolved Raman spectroscopy of single-and few-layer graphene," Nano Lett, vol. 7, p. 238, 2007. https://doi.org/10.1021/nl061702a.

[27]. R. Nallendran, G. Selvan and A.R. Balu, "CdO-$Fe_3O_4$ nanocomposite with enhanced magnetic and photocatalytic properties," Mater. Sci. Poland, vol. 37, p. 100,2019. https://doi.org/10.2478/msp-2019-0012.

[28]. J. Srivind, V.S. Nagarethinam, M. Suganya, S. Balamurugan, K. Usharani and A.R. Balu, "NiO coupled $SnS_2$ nanoparticles with improved magnetic and photocatalytic performance against the degradation of organic dyes without N=N double bond," Vacuum, vol. 163, p. 373, 2019. https://doi.org/10.1016/j.vacuum.2019.02.048.

[29]. R. Nallendran, G. Selvan and A.R. Balu, "Photocatalytic performance of $SnO_2$ Coupled CdO Nanoparticles Against MY and RhB Dyes," J. Electron. Mater, vol. 48, p. 3676, 2019. https://doi.org/10.1007/s11664-019-07125-6.

[30]. G. Williams and P.V. Kamat, "Graphene-Semiconductor nanocomposites: Excited-State interactions between ZnO nanoparticles and graphene oxide," Langmuir, vol. 25, p. 13867, 2009. https://doi.org/10.1021/la900905h.

[31]. J. Xiao,W. Lv, Z. Xie, Y. Tan, Y. Song and Q. Zheng, "Environmentally friendly reduced graphene oxide as a broad spectrum adsorbent for anionic and cationic dyes: via π-π interactions," J. Mater. Chem, vol. 4, p. 12126, 2016. https://doi.org/10.1039/C6TA04119A.

[32]. D. Akyuz, "rGO-$TiO_2$-CdO-ZnO-Ag photocatalyst for enhancing photocatalytic degradation of methylene blue," Opt. Mater, vol. 116, p. 111090, 2021. https://doi.org/10.1016/j.optmat.2021.111090.

[33]. X.S. Li, Q. Wang, Y.B. Zhao, W. Wu, J.F. Chen and H. Meng, "Green synthesis and photocatalytic performances for ZnO - reduced graphene oxide nanocomposites," J. Coll. Interface Sci, vol. 411, p. 69,2013. https://doi.org/10.1016/j.jcis.2013.08.050.

[34]. G. Cheng, F.F. Xu, J.Y. Xiong, F. Tian, J. Ding, F.J. Stadler and R. Chen, "Enhanced adsorption and photocatalysis capability of generally synthesized $TiO_2$-Carbon materials hybrids," Adv. Powder Technol, vol. 27, p. 1949, 2016. https://doi.org/10.1016/j.apt.2016.06.026.

[35]. A. Irshad, F. Farooq, M.F. Warsi, N. Shaheen, A.Y. Elnaggar, E.E. Hussein, Z.M. El-Bahy and M. Shahid, "Ag-doped $FeCo_2O_4$ nanoparticles and their composite with flat 2D reduced graphene oxide sheets for photocatalytic degradation of colored and colorless compounds,"Flatchem, vol. 31, p. 100325.2022. https://doi.org/10.1016/j.flatc.2021.100325.

[36]. S. Kumar, A.K. Ojha and B. Walkenfort, "Cadmium oxide nanoparticles grown in situ on reduced graphene oxide for enhanced photocatalytic degradation of methylene blue dye under ultraviolet irradiation," J. Photochem. Photobiol. B. Bio, vol. 159, p. 111, 2016. https://doi.org/10.1016/j.jphotobiol.2016.03.025.

[37]. A. Allahbaksh, Z. Jarrahi, G. Farzi and A. Shavandi, "Three-dimensional nanoporous Cu-BTC/graphene oxide nanocomposites with engineered antibacterial properties synthesized via a one-pot solvosonication process," Mater. Chem. Phys, vol. 277, p. 125502.2022. https://doi.org/10.1016/j.matchemphys.2021.125502.

[38]. M. Karthika, A.R. Balu, G. Vinitha, Z. Delci, M. Suganya, S. Chitra Devi, K. Devendran and M. Sriramraj, "Electrochemical third order nonlinear optical and antibacterial properties of chitosan, a cationic polymer loaded CuS:Co nanoparticles," Ceram. Int, vol. 49,p. 17806, 2023. https://doi.org/10.1016/j.ceramint.2023.02.146.

[39]. M. Karthika, A.R. Balu, M. Suganya, S. Chitra Devi, M. Sriramraj, K. Devendran, G. Vinitha, Z. Delci and S. Balamurugan, "Chitosan a Cationic Polymer-Loaded CuS:Ni Nanoparticles Well Suited for Pseudocapacitors, Optical Switching and Spintronic Devices," Nano, vol. 18, p. 2350014.2023. https://doi.org/10.1142/S1793292023500145.

[40]. A. Ceril Jeoffrey, S. Jothi Ramalingam, K. Murugaiah and A.R. Balu, "Photocatalytic and antibacterial properties of one pot green synthesized rGO-ZnO/SnO nanocomposite using *Alternanthera sessilis* leaf extract," Inorg. Chem. Commun, vol. 151, p.110585, 2023. https://doi.org/10.1016/j.inoche.2023.110585.

[41]. A. Ceril Jeoffrey, S. Jothi Ramalingam, K. Murugaiah and A.R. Balu, "Highly photoactive rGO-$MnO_2$/CuO nanocomposite photocatalyst for the removal of metanil yellow dye and bacterial resistance against *Pseudomonas Aeruginosa*," Chem. Phys. Impact, vol. 6, p. 100246, 2023. https://doi.org/10.1016/j.chphi.2023.100246.